Free-standing, microscale, mode-selective photonic lantern supported by a truss structure

Yoav Dana,[*] Yehudit Garcia, and Dan M. Marom

Department of Applied Physics, Hebrew University of Jerusalem
Jerusalem, Israel

[*]*yoav.dana@mail.huji.ac.il*

Abstract: We design, fabricate and characterize a three-mode selective photonic lantern using 3D waveguides made of photopolymer core and air cladding. Although the waveguides exhibit high index contrast, cross-talk between mode groups measures below -10dB.

1. Introduction

Photonic lanterns consist of an adiabatic spatial transition from a multi-mode (MM) optical waveguide to a discrete set of single-mode (SM) waveguides, with matching mode and waveguide counts [1]. They can losslessly convert from the MM domain to the SM array domain and are an enabling technology for mode division multiplexing [2]. Photonic lanterns can be made by fibers that coalesce to one [3] and by waveguide inscription in glass using direct laser writing [4]. Due to the adiabatic transition requirement, photonic lantern (PL) devices are typically long and utilize low index contrast waveguides. The ability to 3D print optical waveguides in a photopolymer using direct laser writing [5] results in air-cladded structures having large refractive index contrast and very small transverse dimensions to remain SM. In [6] the design of a three-mode selective PL was reported. This work expands on our previous work by adding the tapers for interfacing to I/O fibers and introducing a mechanical support structure to stabilize the 3D printed PL without introducing any performance degradation.

2. Device Description and Optimization

The SM sources in this work have an MFD of $6\mu m$ and $35\mu m$ pitch, which are to be interfaced to a three-mode fiber on the other end of the PL over $300\mu m$ length disposed in between. The 3D printed waveguides exhibit a high refractive index contrast between core ($n_{core} = 1.53$) and cladding (air at $n_{clad} = 1$), therefore the three-mode waveguide size is $1.6\mu m$ diameter and SM waveguide is $1\mu m$ diameter, at wavelength $\lambda = 1.55\mu m$ ($V = 3.75$ and 2.35, respectively). The PL contains three parts (Fig. 1-a): waveguides to match between the source modes and positions to multiplexer inputs, three mode selective multiplexer (MUX), and an output taper to match between the MUX output to a three mode fiber. Each part has been designed separately. In order to design a mode selective MUX, the input SM waveguides are arranged in a right angled isosceles triangle (Fig. 1-b), with the two waveguides at the acute angles having the same diameter $D_G^{(2)}$ and destined to excite the second mode group and the waveguide at the right angle corner of diameter $D_G^{(1)}$ for fundamental mode excitation, where $D_G^{(2)} < D_G^{(1)}$. Due to the high-index contrast waveguides, mode matching from the sources to the mode size of the MUX's inputs is required. Tapering down the waveguides from the source ($8.4\mu m$ diameter) to a SM diameter ($1\mu m$) and then expanding them to a three-mode diameter ($1.6\mu m$) by using the MUX designed at [6] will required long structure with small diameter waveguides and in practice the fabricated structure will be too fragile and mechanically unstable. Instead, in the current design, the source modes are tapered down to the multiplexer input diameters $D_G^{(1)}$ and $D_G^{(2)}$. Then, the waveguides continue reducing gradually to the three-mode diameter at the MUX's output. The challenge here is preventing the excitation of higher order modes. The mode matching taper ("Transition from source mode" in Fig. 1-a) is optimized to output the fundamental mode with high purity (96%). Then, the MUX is optimized assuming SM inputs. Designing of the MUX requires time consuming FDTD simulations. To calculate the IL, XT and MDL a 6×6 coupling matrix needs to be calculated, and requires performing 6 FDTD simulations. Due to the MUX symmetry, we devised an objective function for minimizing both XT and IL and reduced the number of simulations to two only. Sampling at random a source mode from group 1 ($G^{(1)}$), we launch the sampled mode through in_1 (Fig. 1-b) input waveguide and calculate the coupling coefficients of the MUX's output field with its 6 eigen modes. Let PG^1 be the sum of the overlap coefficients of $G^{(1)}$ (total output power transmitted to mode group 1) and let P_1 be the sum of all 6 coefficients (total output power). Similarly, PG^2 and P_2 are generated by launching a sampled mode source from one of the group 2 ($G^{(2)}$) input waveguides (in_2 or in_3).

The objective function is defined by:

$$\hat{F} = \frac{1}{1+\lambda} \cdot \frac{2PG^1 + 4PG^2}{6} + \frac{\lambda}{1+\lambda} \cdot \frac{2P_1 + 4P_2}{6} \leq 1 \tag{1}$$

The first term of $\hat{F}$ targets crosstalk reduction and the second term maximises the total power transmission. If λ is small ($0 \leq \lambda \leq 1$), the optimization will be more biased towards crosstalk reduction and efficiency may be low. After few experiments we chose $\lambda = 0.4$. $D_G^{(2)}$, $D_G^{(1)}$, MUX length (L) and 20 additional path defining parameters (Fig. 1-a) are optimized with a genetic algorithm (GA) to maximize our objective function $\hat{F}$ as described in [5]. From the optimization, $D_G^{(1)} = 2.2\mu m$ and $D_G^{(2)} = 2.1\mu m$ (Fig. 1-b). To match the PL output to a three-mode fiber, we designed a $90\mu m$ long taper, starting from $1.6\mu m$ diameter (3-mode cross-section) and ending with $16\mu m$, giving a total device length of $340\mu m$. The 3D printing process we use has a limitation of $300\mu m$ in the longitudinal direction for a single print. Therefore, fabricating the complete $340\mu m$ design requires printing the first $300\mu m$ and then, print an additional $40\mu m$ on top of the first part. In this work, we fabricated and characterized the first $300\mu m$ only. The diameter of the output cross-section in this case is $6\mu m$ (supporting 200 modes).

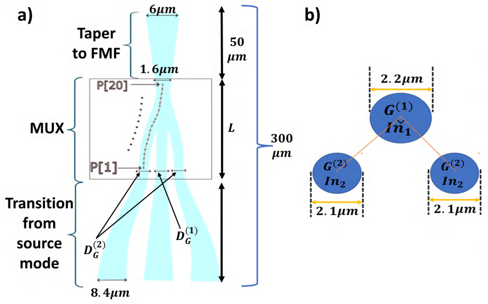

c)

Input	Crosstalk	Efficiency [%]
In_1^x	Group 1 to 2: 16.51 dB	91
In_1^y	Group 1 to 2: 16.71 dB	94
In_2^x	Group 2 to 1: 18.69 dB	85
In_2^y	Group 2 to 1: 19.7 dB	87
In_3^x	Group 2 to 1: 18.17 dB	81
In_3^y	Group 2 to 1: 17.8 dB	88

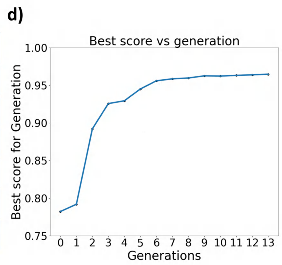

Fig. 1. a) PL structure with its dimensions, optimization parameters and separation to its three parts: Taper to match the source mode to the MUX input mode, three-mode multiplexer (MUX) and a taper to expand the MUX's output mode size. b) MUX input waveguides arrangement and dimensions. c) Simulation results of the XT and total efficiency for each of the PLs inputs. d) Best score in each of the GA generations.

3. Simulations and Fabrication

We performed the GA optimization procedure, improving the objective metric $\hat{F}$ at every generation (Fig. 1-d). The best design for the MUX achieved $IL = -0.22$dB and $XT < -17$dB with minimum value of $XT = -19.8$dB. Although The MUX designed in [6] achieved $IL = -0.14$dB and $XT < -20$dB, it is $20\mu m$ longer and has $1\mu m$ input waveguide diameter, making its fabrication less feasible. By including the source interface waveguides and the output taper the PL achieves $IL = -0.55$dB and $XT < -16.5$dB (Fig.1-c). The PL was first printed on a glass substrate (Fig. 2-a). The PL bent due to a relatively large longitudinal dimension of the structure. To solve it and improve the mechanical stability of the PL, additional external support structure was added to the design (Fig.2-b). The support is connected to the PL only at the output cross section with a $1\mu m$ thin hollow dome (Fig.2-c). Since the dome and the output waveguide taper are connecting with a thin layer of polymer, the optical performance penalty is negligible according to our simulations.

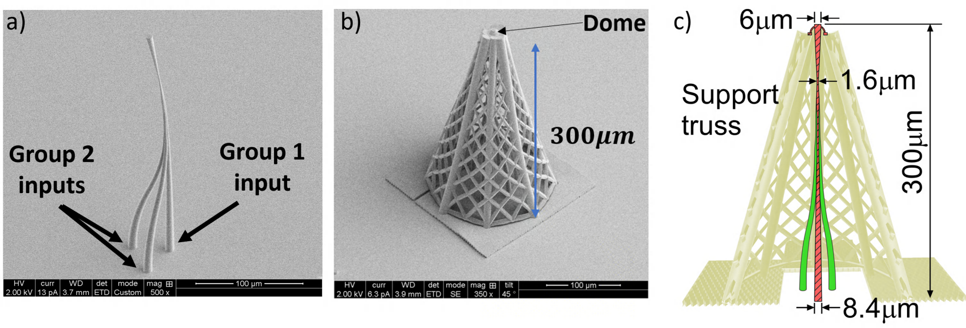

Fig. 2. a) Fabricated three-mode selective PL. b) Fabricated 3-mode PL with a support structure. c) Cross-section view through CAD model of PL + supporting truss section.

4. Characterization

To measure the PL's transfer matrix, we used off-axis digital holography (DH) for measuring the complex electric field of the device's output. Then, by performing digital demultiplexing with 6 simulated digital modes (3 modes with 2 polarization states) we measure the transfer matrix and calculate the IL, MDL and XT. The whole procedure described in [5, 7]. The measured transfer matrix absolute squared is shown in Fig. 3-a. By eigen value decomposition, an IL of -1.13dB and MDL of -2.21dB were measured. The XT between mode groups is lower than -10dB with a minimum value of -19dB. To make sure that higher order modes are not excited, we performed mode decomposition with 10 higher order modes. The highest coupling value was less than -20dB. Fig. 3-b shows polarization resolved, electric field outputs of the PL with different input excitations. As expected, an excitation from the wide waveguide generated a field profile similar to the LP_{01} mode (group 1). Excitation from the narrower inputs generated a profile more similar to the $LP_{11}^{a\backslash b}$ (group 2). In addition, we measured the optical output power of the PL directly with a power meter, over a wavelength band of [1520-1600]nm (Fig.3-c). The fundamental mode input (In_1) outperform the other two by $\sim 2dB$ over the entire band. One explanation for the difference, as shown in Fig.2-a, the input waveguides for group 2 has larger displacement S-shaped curves. Furthermore, fabrication imperfections such as waveguides size, alignment to the source and surface roughness affect the loss as well. The power measurement done for two orthogonal polarization states at each input, and as shown in Fig.3-c the difference between polarization is relatively small. The efficiency for all inputs of the PL increases by $\sim 1dB$ across the wavelength band with the highest efficiency measured when $\lambda = 1600$nm. Our assumption is that the dominant loss mechanism in this case is scattering, with shorter wavelengths being more susceptible to scattering. This assumption needs to be further examined.

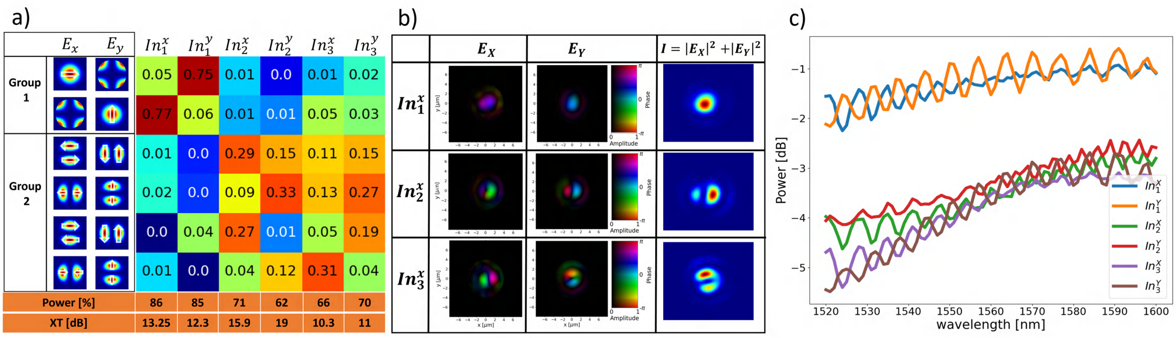

Fig. 3. a) Measured Transfer matrix absolute squared. $In_i^{x/y}$ are representing the PLs input modes from waveguide i with polarization components x or y. b) Output fields (two transverse components and intensity) of the PL with different inputs. c) Direct power measurement for all 6 inputs of the PL, at wavelength range of $[1520-1600]$nm.

5. Conclusions

We demonstrated the feasibility of shrinking a three-mode selective photonic lantern to multi-micron scale, based on high refractive index waveguides, while retaining cross-talk between mode groups below -10dB, with IL of -1.13dB and MDL of -2.21dB. Simulation results shows XT below -16.5dB with IL of -0.55dB. The main cause for the difference is likely fabrication imperfections. In the future, we will complete the output taper to directly couple to a three-mode fiber and conduct system experiments.

References

1. T. A. Birks, et al., "The photonic lantern," Adv. Opt. Photon. 7(2), 107-167 (2015).
2. N. K. Fontaine, et al., "Geometric requirements for photonic lanterns in space division multiplexing," Opt. Express 20(24), 27123-27132, 2012.
3. S. G. Leon-Saval, et al., "Multimode fiber devices with SM performance," Opt. Letters 30(19), 2545-47, 2005.
4. R. R. Thomson, et al., "Ultrafast laser inscription of an integrated photonic lantern," Opt. Express 19(6), 5698-5705, 2011.
5. Y. Dana and D. M. Marom, "Microscale six-mode photonic lantern multiplexer compatible with 3D nanoprinting technology," International Conference on Optical MEMS and Nanophotonics (OMN) 2022, 2022.
6. Y. Dana and D. M. Marom, "Microscale mode-selective photonic lantern multiplexer compatible with 3D nanoprinting technology," Optical Fiber Communication Conference (OFC) 2022, Th2A.6, 2022.
7. S. Van Der Heide, et al., "Exploiting Angular Multiplexing for Polarization-diversity in Off-axis Digital Holography," 2020 European Conference on Optical Communications (ECOC), pages 1-4, 2020.